

# Optimization of Pressure Vessel Under Thermo-Elastic Condition

Nayan Jyoti Baishya · Deepak Sharma\* · Uday S. Dixit

Received: date / Accepted: date

**Abstract** In this paper, a pressure vessel under thermo-elastic condition is modeled which is useful for industries like refineries, power plant etc. The combined effect of internal pressure and steady-state temperature gradient is considered. A pressure vessel problem is formulated to minimize its total cost subjected to constraints that can ensure safe design. The problem is solved using elitist genetic algorithm. Further simulations on stress versus thickness are carried out which reveal that the maximum shear stress gets reduced up to a certain thickness. After that, it starts increasing due to increase in the compressive hoop/circumferential stress under thermo-elastic condition. The bi-objective optimization problem is then formulated by minimizing the total cost and the maximum shear stress simultaneously. The bi-objective problem is solved using elitist non-dominated sorting genetic algorithm. The cost effective to the safe trade-off solutions are generated. These approximate Pareto-optimal solutions are evolved in two clusters in which solution from one of the clusters is more preferable for practical and feasible pressure vessel design. The post-optimization analysis of results suggests that the bi-objective optimization study offers valuable insight of the problem than the single-objective optimization.

**Keywords** Pressure Vessel Design Optimization · Engineering Optimization · Thermo-Elastic Condition

---

\*Corresponding author. Email: dsharma@iitg.ernet.in

Department of Mechanical Engineering,  
Indian Institute of Technology Guwahati,  
Assam, India, PIN-781039,  
E-mail: {n.baishya, dsharma, uday}@iitg.ernet.in

## 1 Introduction

A pressure vessel is a closed container which is designed to carry liquids/gases at a pressure different than atmospheric pressure. It is useful for industries like refineries, power plants, fertilizer plants etc. Depending on its use, it can be designed to operate safely for a specific pressure and temperature. For example, a pressure vessel under thermo-elastic condition serves a purpose of closed container for hot fluid/gas and also, is subjected to internal pressure. Severe safety measures are generally considered for designing it in order to avoid failures and accidents. However in a scenario of limited and expensive raw material, its safe and optimal design is desirable to minimize its total fabrication cost.

In general, the pressure vessels are designed using various codes used in different countries such as ASME Boiler and Pressure Vessel code section VIII in U.S.A., PD 5500 in U.K., MITI code in Japan etc. The purpose of these codes is to design safe pressure vessel by preventing failure or accidents. For example in ASME code, the pressure vessel design guidelines are described in section VIII. The same section is further divided into three divisions. The divisions 1 and 2 are used for pressure vessel having internal or external pressure more than 15 psi and temperature lying between  $-29^{\circ}\text{C}$  and  $345^{\circ}\text{C}$ . The division 1 is based on rules in which factor of safety (FOS) is considered as 4. The division 2 is based on analysis and rules in which FOS is reduced to 3. The rules of division 1 are specified for minimum requirements to design a pressure vessel. However, the finite element method in addition to the analytical approach of design by formula are used for division 2. The division 3 is used for high pressure design when pressure is more than 10,000 psi. Interested reader can refer [26, 1] for more detail.

In case of a pressure vessel subjected to internal pressure, the maximum shear stress ( $\tau_{max}$ ) gets reduced with increase in thickness of a sheet and it is developed at the inner wall. However, the cost of fabrication keeps on increasing. But in a pressure vessel subjected to thermo-elastic condition,  $\tau_{max}$  can be observed anywhere along the thickness of a sheet [12,11] due to the combined effect of internal pressure and temperature gradient. It is shown later in this paper that  $\tau_{max}$  gets reduced with increase in thickness up to a certain value and then it starts increasing. Therefore, it is essential to design an optimal pressure vessel.

In the literature, an optimization problem was formulated for a pressure vessel where the design codes were used to formulate the objective function and constraints. A non-linear, mixed variable and discrete programming was formulated [31] in which the fabrication cost was minimized by limiting volume and length of a cylinder. The branch and bound method with exterior penalty function was used to find the optimal value of parameters. The same problem was further solved using augmented Lagrange multiplier method coupled with Powell's method, and Fletcher and Reeves conjugate gradient method [18], logarithmic method [22] etc. The motive was to find the optimal or near optimal value of parameters that can minimize the fabrication cost.

The non-tradition optimization algorithms were also used to improve the existing solution. For example,  $(1 + \lambda)$  Evolution Strategy [25], genetic algorithm (GA) [4], infeasibility based evolutionary algorithm [24], filter simulated annealing method [17], ant colony optimization with chaotic sequence [3], artificial bee colony [34], particle swarm optimization (PSO) [29,13,27,2,15] etc. were used. The hybrid optimization algorithms were also employed to generate near optimal results such as hybrid GA [30], Nelder-Mead simplex method with PSO [36], quasi-Newton and conjugate gradient methods with PSO [19] to name a few.

Earlier, it has been shown by many researchers that solving single-objective optimization (SOO) problem as multi-objective optimization can generate better solutions. It was termed as "multi-objectivization" [21] in which a multi-objective problem is formulated by adding the conflicting secondary objective(s) with the primary objective. The multi-objectivization can introduce adequate diversity in evolutionary multi-objective optimization (EMO) procedure, thereby allowing EMO to find good solutions. In the literature, multi-objectivization concept has been used in many studies like traveling salesman problems [21], structure optimization [32,33] etc.

In this paper, the modeling of a pressure vessel subjected to thermo-elastic condition is developed. A pres-

sure vessel is designed for its minimum total cost ( $TC$ ). The constraints on stress, volume and length are imposed for safe and optimal design. The optimization problem is then solved using elitist GA (eGA) and also using the branch and bound method with `fmincon()` function in Matlab [23]. The simulation results are presented to show the optimal solution and behavior of  $\tau_{max}$  with thickness under thermo-elastic condition. Thereafter, the bi-objective optimization problem of a pressure vessel is solved using elitist non-dominating sorting genetic algorithm (NSGA-II). The remaining paper is organized as follows. In Section 2, the modeling of pressure vessel under thermo-elastic condition is presented. The objective function and constraints are formulated and explained. The two optimization procedures for SOO and NSGA-II for the bi-objective optimization problem are discussed in Section 3. The simulation results are presented, compared and discussed in Section 4. The paper is concluded in Section 5 with the direction for future work.

## 2 Modeling of Pressure Vessel Under Thermo-Elastic Condition

In this section, the objective function and constraints are modeled for a pressure vessel under thermo-elastic condition. Following assumptions are considered in this paper:

1. The cylindrical shell is under plane stress condition.
2. External pressure is very small in comparison to internal or gauge pressure.
3. Temperature does not vary with time.
4. Material properties do not change with temperature.
5. Weld joint joining spherical head and cylindrical shell is very strong and no failure can take place at the joint.
6. Same density is assumed for welding and pressure vessel material.

### 2.1 Single Objective Function

A pressure vessel is modeled to minimize its  $TC$ . It consists of the welding and material costs which depends on the design of a pressure vessel. In this paper, a pressure vessel with two hemi-spherical heads attached to both ends of a cylindrical shell is considered as shown in Fig. 1. The welding cost of this pressure vessel is calculated by welding the two rolled sheets to make a cylindrical shell using  $60^\circ$  single V-groove butt joint as shown in Fig. 2 (a). It is approximated as one-sixth sector of a circle of radius  $(T_s / \cos 30^\circ)$  as shown in Fig. 2

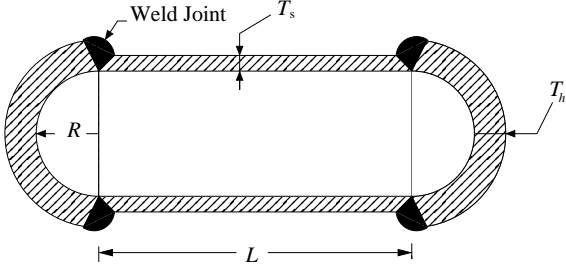


**Fig. 1** A cross sectional view of a pressure vessel in which two hemi-spherical heads are welded to a cylindrical shell.

(b). A variable set used for modeling a pressure vessel

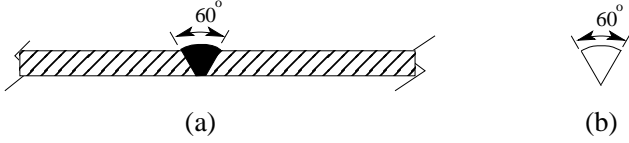


**Fig. 2** Welding details of 60° single V-groove butt joint (a) actual profile (b) approximate profile.

is  $\bar{x} = [T_s, T_h, R, L]^T$ . The variables  $T_s$  and  $T_h$  signify thickness of sheet used for fabricating cylindrical shell and hemi-spherical heads. Generally, the standard sizes of sheet thickness are available in the market thereby making these variables discrete in nature. Other two variables are real continuous parameters.

The cost of longitudinal weld for a cylindrical shell is given as [31]

$$C_1 = 2\pi\rho LC_w \left( \frac{T_s}{\cos 30^\circ} \right)^2 \left( \frac{60^\circ}{360^\circ} \right), \quad (1)$$

where “2” signifies welding of two rolled sheets longitudinally at two places to make a cylindrical shell, “ $\pi(T_s/\cos 30^\circ)^2(60^\circ/360^\circ)$ ” represents area of one-sixth sector of a circle, “ $\rho$ ” is the density,  $C_w$  is the cost of weld material per kg.

The hemi-spherical heads are forged and welded to the ends of a cylindrical shell using same butt joint as shown in Fig. 2. The cost of welding spherical heads to a cylindrical shell is given by [31]

$$C_2 = 4\pi^2\rho RC_w \left( \frac{T_h}{\cos 30^\circ} \right)^2 \left( \frac{60^\circ}{360^\circ} \right). \quad (2)$$

Here, “ $\pi(T_h/\cos 30^\circ)^2(60^\circ/360^\circ)$ ” represents area of one-sixth sector of a circle, and “ $R$ ” is radius of spherical head.

The total material cost of pressure vessel is given as [31]

$$C_3 = 2\pi\rho RLT_s C_s + 4\pi\rho R^2 T_h C_h. \quad (3)$$

$TC$  of a pressure vessel is  $(C_1 + C_2 + C_3)$ . The objective is to minimize  $TC$  which is a non-linear function of four variables. In the following section, various constraints are discussed for safe and optimal design.

## 2.2 Constraints

In this section, the constraints are discussed which can ensure a safe design and required capacity.

1. Volume constraint: It signifies a minimum capacity/volume for a pressure vessel. Here, it is assumed that the volume should be more than 50 cubic meter. Mathematically, the volume constraint is expressed by

$$g_1(\bar{x}) = \pi R^2 L + \frac{4}{3}\pi R^3 - 50.0 \geq 0. \quad (4)$$

2. Width constraint: It signifies a limit on the width of a sheet influenced by the capacity of rolling equipment. Here it is assumed that the width should be less than 600 mm. The width constraint in mathematical form is given as

$$g_2(\bar{x}) = 600 - L \geq 0. \quad (5)$$

3. Stress constraint: This constraint is responsible for a safe design by limiting  $\tau_{max}$  developed in a pressure vessel which is given as

$$g_3(\bar{x}) = \tau_{max} < \sigma_y/2. \quad (6)$$

$\tau_{max}$  developed in a 3-D body is obtained by using maximum shear stress theory (Tresca theory), i.e., shear stress developed in a body in the presence of three perpendicular stresses is given as

$$\tau = \frac{\max(\sigma_{rr}, \sigma_{\theta\theta}, \sigma_{\phi\phi}) - \min(\sigma_{rr}, \sigma_{\theta\theta}, \sigma_{\phi\phi})}{2}. \quad (7)$$

$\tau_{max}$  is then calculated as  $\tau_{max} = \max\{\tau_{shell}, \tau_{sphere}\}$  where  $\tau_{shell}$  and  $\tau_{sphere}$  are calculated from (7) for a cylindrical shell or spherical head, respectively. For cylindrical shell, the radial and hoop stresses due to thermo-elastic stresses [28] are given as

$$\sigma_{rr} = \frac{pR^2}{((R+T_s)^2 - R^2)} \left( 1 - \frac{(R+T_s)^2}{r^2} \right) + \frac{\alpha E}{2} (T_b - T_a) \times \left[ -\frac{\ln \frac{r}{R}}{\ln \frac{(R+T_s)}{R}} + \left( 1 - \frac{R^2}{r^2} \right) \frac{(R+T_s)^2}{((R+T_s)^2 - R^2)} \right], \quad (8)$$

$$\sigma_{\theta\theta} = \frac{pR^2}{((R+T_s)^2 - R^2)} \left( 1 + \frac{(R+T_s)^2}{r^2} \right) + \frac{\alpha E}{2} \times (T_b - T_a) \times \left[ -\frac{1 + \ln \frac{r}{R}}{\ln \frac{R+T_s}{R}} + \left( 1 + \frac{R^2}{r^2} \right) \frac{(R+T_s)^2}{((R+T_s)^2 - R^2)} \right], \quad (9)$$

where “ $p$ ” is internal or gauge pressure, “ $r$ ” is an arbitrary radius between  $R$  and  $R + T_s$ , “ $\alpha$ ” is coefficient of thermal expansion, “ $E$ ” is modulus of elasticity, “ $T_a$ ” is inside temperature and “ $T_b$ ” is outside temperature.

For spherical head, the radial and hoop stresses under thermo-elastic condition [28] are given as

$$\sigma_{rr} = \frac{pR^3}{((R+T_h)^3 - R^3)} \left( 1 - \frac{(R+T_h)^3}{r^3} \right) - \frac{\alpha E}{1-\nu} (T_b - T_a) \frac{R(R+T_h)}{(R+T_h)^3 - R^3} \left( 1 - \frac{R}{r} \right) \left( 1 - \frac{R+T_h}{r} \right) \left( 2R+T_h + \frac{R(R+T_h)}{r} \right), \quad (10)$$

$$\sigma_{\theta\theta} = \sigma_{\phi\phi} = \frac{pR^3}{((R+T_h)^3 - R^3)} \left( 1 + \frac{(R+T_h)^3}{2r^3} \right) - \frac{\alpha E}{1-\nu} (T_b - T_a) \frac{R(R+T_h)}{(R+T_h)^3 - R^3} [2R+T_h - ((R+T_h)^2 + R(R+T_h) + R^2) \frac{1}{2r} - \frac{R^2(R+T_h)^2}{2r^3}], \quad (11)$$

Except (5), all constraints are non-linear which are designed using four mixed variables.

### 2.3 Multi-Objective Problem Formulation

Motivated from the concept of “multi-objectivization”, SOO problem of a pressure vessel is converted to the bi-objective optimization which is given as

$$\begin{aligned} &\text{Minimize: } TC \text{ of pressure vessel} \\ &\text{Minimize: } \tau_{max} \text{ developed in the pressure vessel,} \end{aligned} \quad (12)$$

$TC$  is evaluated as described in Section 2.1 and  $\tau_{max}$  is calculated from (7). The bi-objective optimization problem is subjected to same constraints as defined in Section 2.2.

In the following section, the two optimization methods for SOO and one multi-objective optimization algorithm are discussed which are used to solve pressure vessel design optimization problems.

## 3 Optimization Procedures

### 3.1 SOO Procedures

The two optimization procedures are used for solving the given optimization problem for a pressure vessel. First optimization method is based on the branch and bound method in which a non-linear programming (NLP) problem is solved using `fmincon()` function of Matlab. A flow chart of hybrid algorithm is shown in Fig. 3 in which a NLP problem is solved by considering all variables as real using `fmincon()` function. The value of parameters are then supplied to the branch and bound method in which value of discrete integer variables is fathomed. For unfathomed variables, the standard procedure of the branch and bound method is followed and a NLP problem is solved using `fmincon()` function. The hybrid algorithm terminates when all integer variables become fathomed. The termination for `fmincon()` function is set to  $10^{-6}$  for ‘ $TolX$ ’. Interested readers can refer Matlab documentation for more details on termination condition. The source code of this hybrid algorithm can be found at [35].

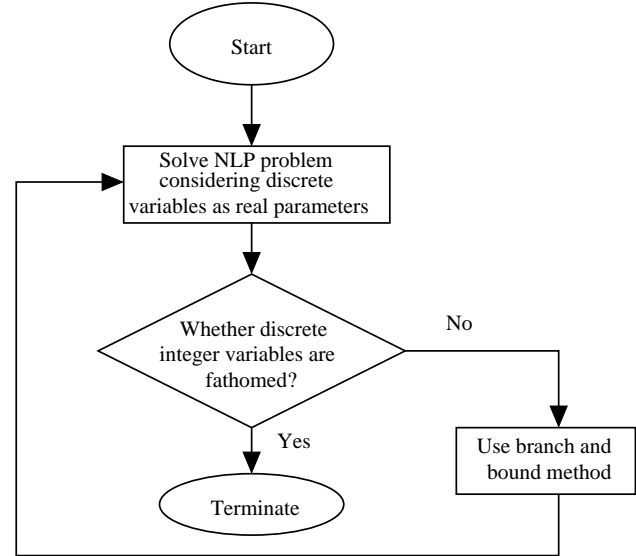


**Fig. 3** A flow chart of hybrid algorithm in which branch and bound method is used. For solving NLP problem, `fmincon()` function of Matlab is used.

Another method used for solving the same optimization problem of a pressure vessel is eGA. The flow chart of algorithm is shown in Fig. 4 in which a population is generated randomly. The population is then evaluated and the fitness is assigned using the constraint handling technique proposed in [5]. In the fitness assignment, a better fitness is assigned to a feasible solution than any infeasible solution. Thereafter, the termination condi-

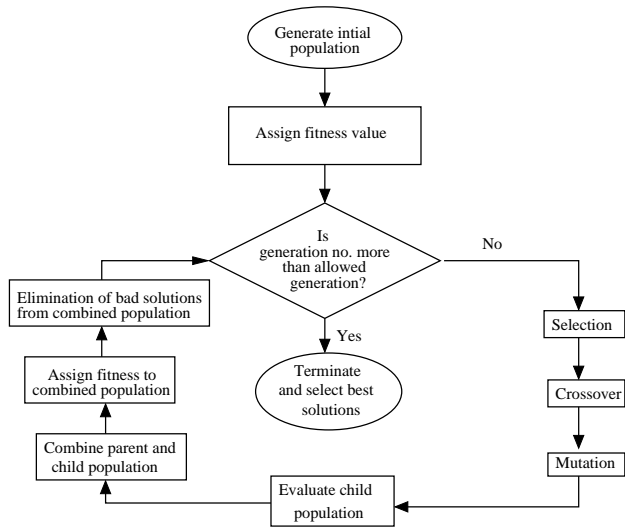


Fig. 4 A flow chart of elitist GA.

tion on maximum generation is checked for GA. If GA does not terminate, then the binary tournament selection operator is applied to the population (which is referred as parent population now) to make a mating pool of good individuals. Interested readers can refer [16] for more details on the tournament selection operator. After creating a mating pool, the crossover is done on randomly chosen parents to create children. The simulated binary crossover (SBX) operator [7] is used which creates two children from two parent solutions. The newly created solutions are now mutated using the polynomial mutation operator [8] to create a new population which is referred as child population. Now, the fitness is assigned to the child population in same manner as explained earlier. An elitist strategy is used with GA in which the parent and child populations are mixed together and the best solutions are chosen to make the parent population for next generation. Rest of the solutions from the combined population are discarded. This completes one generation of GA and it continues till the termination condition gets satisfied. It is worthwhile to mention that the discrete variables are handled as real parameters. For example, if eGA evolves real value of 4.3 for  $T_s$ , then the value of  $T_s$  saved at fourth position (nearest integer to 4.3) of array as shown in Fig. 5 is assigned, that is,  $T_s = 6$  mm.

$T_s =$	2	3	5	6	8	10
---------	---	---	---	---	---	----

Fig. 5 An array representation for thickness of a sheet.

### 3.2 Multi-Objective Optimization Algorithm

NSGA-II proposed in [10] is used for solving the bi-objective optimization problem of a pressure vessel. Primarily reason of choosing NSGA-II over other algorithms is that NSGA-II has shown a good convergence and diversity properties to the global Pareto-optimal (P-O) front for various two-objective test and engineering optimization problems [6]. The flow chart of NSGA-II is same as Fig. 4. The fitness is assigned using the non-dominated sorting ranking and the crowding distance operator. The constraint tournament operator is used at selection and elimination stages in which a solution with lower rank and larger crowding distance is preferred. Other operators and discrete variables handling are same as discussed with eGA. Interested readers can refer [10] for more details on NSGA-II.

The two termination conditions are set for NSGA-II. First termination condition gets triggered when the generation counter reaches 1000. Otherwise, the normalized distance ( $ND$ ) metric [9] based condition terminates NSGA-II which is given as

$$ND = \sqrt{\frac{1}{M} \sum_{i=1}^M \left( \frac{z_i^{est} - z_i^*}{z_i^w - z_i^*} \right)^2}. \quad (13)$$

Here, “ $M$ ” is number of objectives, “ $z_i^*$ ” is the ideal point, “ $z_i^w$ ” is the worst point and “ $z_i^{est}$ ” is the estimated Nadir point at any generation of NSGA-II. These points are shown in Fig. 6 for the given P-O front. In

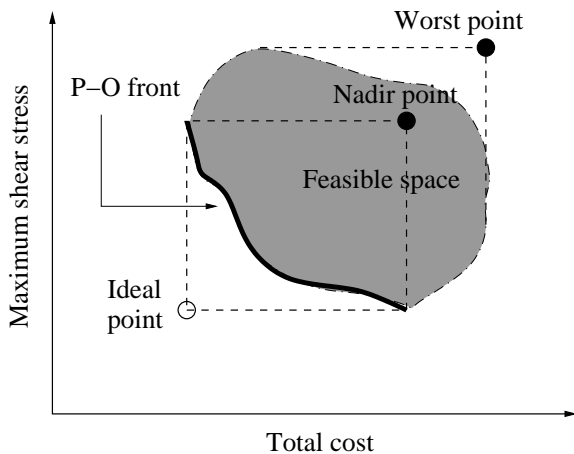


Fig. 6 Ideal point, Nadir point, and worst point in two-objective space of cost and shear stress.

this paper,  $z_i^*$  and  $z_i^w$  are the best ideal and worst points in the population found so far. If value of ideal point and/or worst point of the current generation is better than  $z_i^*$  and/or  $z_i^w$ , then values of  $z_i^*$  and/or  $z_i^w$  get up-

dated.  $z_i^{est}$  can be found from the extreme solutions of the current non-dominated front.

$ND$  values are stored for every generation, and maximum ( $ND_{max}$ ), minimum ( $ND_{min}$ ) and average ( $ND_{avg}$ ) values of  $ND$  are calculated from last 50 generations. When  $\{(ND_{max} - ND_{min})/ND_{avg}\} \leq \Delta$ , then NSGA-II gets terminated.

In the following section, the pressure vessel design problem is solved using three optimization procedures and results are presented and discussed.

## 4 Simulation Results

In this section, the simulation results from SOO methods are presented and compared. The optimal values of variables are perturbed in their vicinity to observe the changes in  $TC$  and  $\tau_{max}$ . The simulation results for capturing behavior of  $\tau_{max}$  developed in a pressure vessel with respect to its thickness are also presented. The bi-objective optimization problem is also solved and compared with SOO study.

### 4.1 SOO Study

In general, the thickness of a sheet available in a market is standard. Following sizes of sheet thickness for fabricating cylindrical shell and spherical heads are assumed to be available:  $\{2, 3, 5, 6, 8, 10, 12, 14, 16, 18, 20, 22, 25, 28, 30, 32, 34, 36, 40, 42, 45, 48, 50\}$  mm. After 50 mm, an increment of 1 mm is considered till 150 mm of thickness. It is noted that the thickness variation may change from country to country. The design parameters considered for solving the pressure vessel optimization problem are shown in Table 1. A few parameters are kept constant for eGA which are given in Table 2.

**Table 1** Design Data used for solving pressure vessel problem

Design parameter	Design data
$C_s$	Rs. 60 per kg
$C_h$	Rs. 80 per kg
$C_w$	Rs. 600 per kg
$P$	$10^5$ Pa
$T_a$	100°C
$T_b$	25°C
Material	Carbon steel (IS 2062 Gr. B)
$\sigma_y$	164 MPa
$E$	210 GPa

In this paper, eGA is tested for different population sizes for solving the given optimization problem. eGA is executed for 20 different runs with different random

**Table 2** eGA parameters.

Crossover probability	: 0.9
Mutation probability	: 0.25
$\eta_c$ for SBX	: 10
$\eta_m$ for polynomial mutation	: 20
Generation	: 100

**Table 3** Statistical values of  $TC$  obtained from 20 different runs of eGA.

Pop- >	8	12	16	20
Best	117976.2	118032.6	117906.4	118261.6
Worst	124063.4	167654.3	122938.8	122811.3
Mean	120883.8	122662.6	119579.8	120317.2
Median	120437.1	119565.9	119358.85	120177.9
Std. Dev.	1897.0	10466.1	1399.7	1485.2

**Table 4** Optimal values of parameters and  $TC$  generated by two optimization methods.

eGA				
$TC$ (Rs)	$R$ (mm)	$L$ (mm)	$T_s$ (mm)	$T_h$ (mm)
117906.4	173.5	297.2	3	3
Hybrid method				
$TC$ (Rs)	$R$ (mm)	$L$ (mm)	$T_s$ (mm)	$T_h$ (mm)
117804.07	175.2	284.7	3	3

initial population for each population size and the results are shown in Table 3. It can be observed that minimum  $TC$  evolved with the population size of 16, although other population sizes show marginally different  $TC$ . The function evaluations required for the population size 16 is 1600. The optimal values of parameters evolved by eGA are shown in Table 4. The same table also shows the optimal values generated by the hybrid method. It can be observed that  $TC$  generated by the hybrid method is marginally better than eGA. Although  $T_s$  and  $T_h$  are evolved with identical thickness values by both the optimization methods, but difference in  $R$  and  $L$  values shows 0.087% improvement in  $TC$  by the hybrid method. The function evaluations required by the hybrid method are 2289 that is more than eGA.

#### 4.1.1 Perturbation Analysis

It can be observed from the last section that the two optimization methods for SOO generated similar solutions. In this section, the optimal value of parameters evolved by the hybrid method are perturbed to observe  $TC$  and  $\tau_{max}$ . Fig. 7 shows that  $TC$  value gets reduced if  $T_s$  is perturbed to 2 mm from its optimal value at 3 mm. However, the design is unsafe because  $\tau_{max}$  becomes greater than  $S = \sigma_y/2$ . Any thickness between 2 mm and 3 mm cannot be chosen due to discrete integer assumption made in section 4.1. For larger values of  $T_s$ ,  $TC$  keeps on increasing but  $\tau_{max}$  gets reduced. From

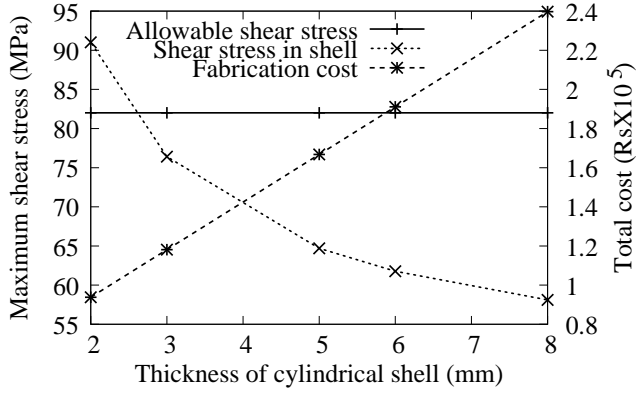


Fig. 7 Variation of  $\tau_{max}$  and  $TC$  with respect to perturbation in  $T_s$ .

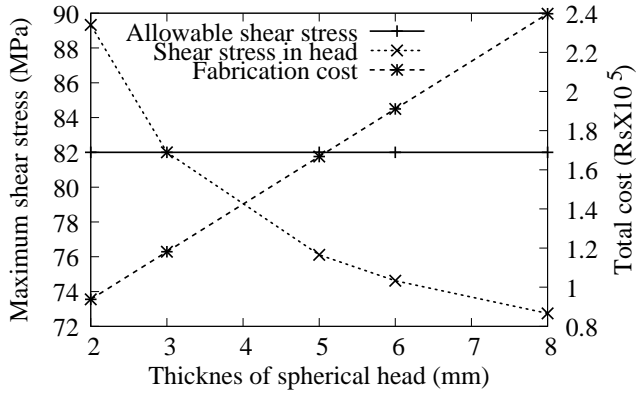


Fig. 8 Variation of  $\tau_{max}$  and  $TC$  with respect to perturbation in  $T_h$ .

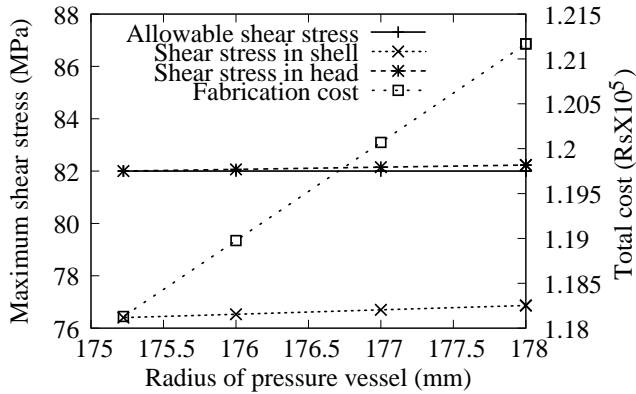


Fig. 9 Variation of  $\tau_{max}$  and  $TC$  with respect to perturbation in  $R$ .

this figure, it can be concluded that 3 mm is an optimal thickness of cylindrical shell for which minimum  $TC$  is achieved.

Similar observation can be seen in Fig. 8 in which  $T_h$  is perturbed. It can be concluded that 3 mm is an optimal value of  $T_h$  for minimum  $TC$ .

Figure 9 shows that  $TC$  and  $\tau_{max}$  keep on increasing with increase in  $R$  value of a pressure vessel. Below

the optimal value of  $R$ , volume constraint is not satisfied. Therefore, the plot is shown for increasing value of  $R$ . At the optimal value of  $R$ ,  $\tau_{max}$  is equivalent to  $S$  thereby making it safe. Any perturbation in  $L$  will not change  $\tau_{max}$ , however volume capacity and  $TC$  will increase.

#### 4.1.2 Behavior of $\tau_{max}$ versus $T_s$ and $T_h$ in a Pressure Vessel

In the preceding section, it has been observed that  $\tau_{max}$  gets reduced with increase in the thickness of cylindrical shell and hemi-spherical heads. However after certain increment of the thickness,  $\tau_{max}$  starts increasing as shown in Figs. 10 and 11 for the cylindrical shell and the hemi-spherical head, respectively. Note that the optimal values of  $R$  and  $L$  evolved by the hybrid method are kept same.

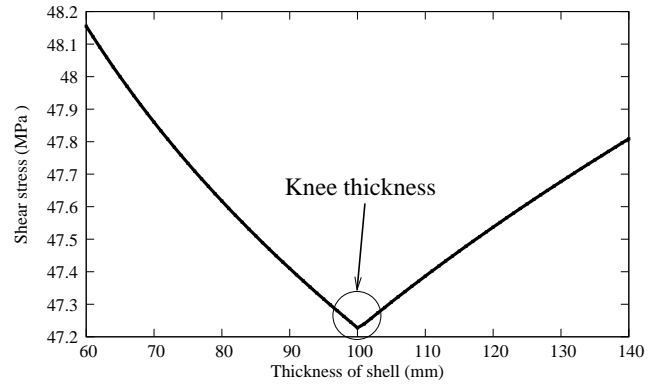


Fig. 10 Variation of  $\tau_{max}$  in a cylindrical shell with respect to its thickness.

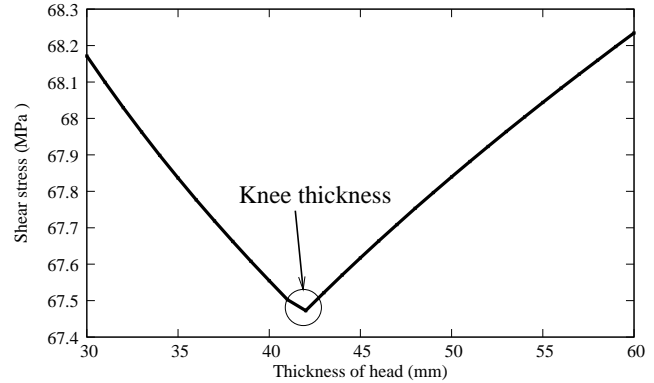


Fig. 11 Variation of  $\tau_{max}$  in a spherical head with respect to its thickness.

The thickness is referred as “knee thickness” from where  $\tau_{max}$  starts increasing. The knee thickness is found at 100 mm for the cylindrical shell and 42 mm for the hemi-spherical head.  $\tau_{max}$  and other stresses observed at and around knee thickness are shown in Table 5. It can be observed that  $\tau_{max}$  gets reduced till

100 mm knee thickness in the cylindrical shell but it starts increasing afterwards. The position of  $\tau_{max}$  also gets shifted from the outer wall to the inner wall. It is due to increase in the compressive hoop stress developed at the inner wall of a cylindrical shell which also starts increasing after the knee thickness under thermo-elastic loading. Similar observation can be seen with the hemi-spherical head in which  $\tau_{max}$  starts increasing after 42 mm knee thickness and the position of  $\tau_{max}$  gets shifted from the outer to the inner wall due to the hoop/circumferential stress under thermo-elastic loading.

**Table 5** Stresses and position of  $\tau_{max}$  at and around knee thickness.

Cylindrical Shell					
$T_s$ (mm)	$\sigma_{rr}$ (MPa)	$\sigma_{\theta\theta}$ (MPa)	$\tau_{max}$ (MPa)	Position of $\tau_{max}$	FOS
99	0	94.490	47.245	Outer wall	1.735
100	0	94.455	47.228	Outer wall	1.736
101	0.1	94.479	47.24	Inner wall	1.735
Spherical Head					
$T_h$ (mm)	$\sigma_{rr}$ (MPa)	$\sigma_{\theta\theta}$ (MPa)	$\tau_{max}$ (MPa)	Position of $\tau_{max}$	FOS
41	0	135.006	67.503	Outer wall	1.214
42	0.1	135.046	67.473	Inner wall	1.215
43	0.1	135.144	67.522	Inner wall	1.214

From last column of Table 5, it is observed that maximum FOS of 1.215 with respect to allowable yield stress of 164 MPa can be achieved by increasing the thickness of pressure vessel under thermo-elastic loading. It also suggests that the hemi-spherical head design is more critical than the cylindrical shell because it shows least FOS value. Figure 8 shows same observation in which  $\tau_{max}$  at the head is equivalent to  $S$  at its optimal value. However in shell,  $\tau_{max}$  is less than  $S$  at its optimal value as shown in Fig. 7.

## 4.2 Multi-Objective Optimization Study

Earlier, the pressure vessel was designed for its minimum  $TC$  subjected to various constraints. In this section, the bi-objective optimization problem defined in (12) is solved using NSGA-II. The same parameter values are used as shown in Tables 1 and 2. The population size is kept 100 for NSGA-II. The algorithm gets terminate when either  $\Delta$  is less than  $10^{-6}$  for ND-values or generation counter reaches 1000.

The algorithm is run for 20 times with different initial population. Figure 12 shows 0% and 50% attainment plots. A brief detail of attainment surface plot is given in appendix A. It is observed that both plots are

completely overlapped to each other. This suggests that NSGA-II is converged to similar sets of the approximate P-O solutions. The main reason is due to the presence of mixed variables in which two are discrete in nature. The same reason is also responsible for gaps in the approximate P-O solutions.

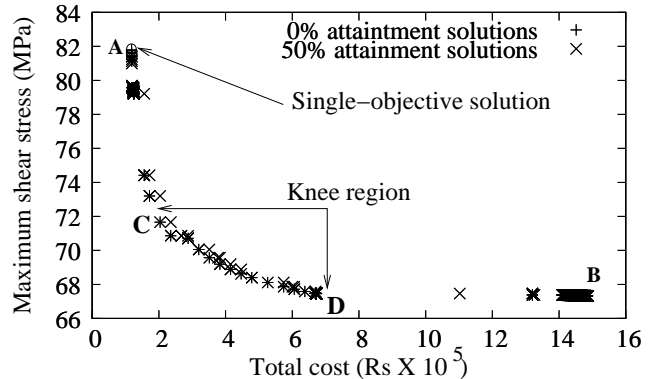


**Fig. 12** Approximate P-O solutions from 20 different runs of NSGA-II.

Figure 12 also shows the optimal solution from SOO study. It can be observed that solution **A** on one extreme of the approximate P-O set shows equivalent  $TC$  of the single-objective optimal solution. Moreover, the bi-objective study evolves other trade-off solutions by simultaneously minimizing  $\tau_{max}$  in the pressure vessel. The outcome from the bi-objective optimization can offer flexibility to the designers to choose an appropriate pressure vessel design from the set of the approximate P-O solutions. For example, the safest solution **B**, the cost effective solution **A** or any trade-off solution can be chosen from the approximate P-O set. It is interesting to note that solution **B**'s thickness (45 mm) is close to the knee thickness shown in Fig. 8. For solutions **B**,  $\tau_{max}$  is 67.3 MPa which is equivalent to  $\tau_{max}$  at the knee thickness. It is worth to mention that the bi-objective study is able to generate all possible solutions from the cost effective solution to the safest design in one run. However with SOO study, further optimization and simulations have to be carried out for similar observations.

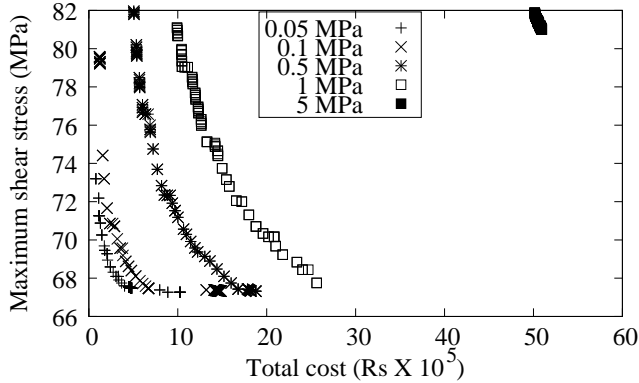
A knee region is observed in Fig. 12 where small gain in one objective implies large compromise in another objective. For example, any improvement in  $\tau_{max}$  against solution **D** drastically increases  $TC$ . Similar observation can be seen against solution **C** in which small gain in  $TC$  implies higher jump in  $\tau_{max}$ . This analysis can be helpful for the designers where relative comparison can be done among the solutions for selecting an appropriate pressure vessel design.

Table 6 shows statistical values of function evaluations for 20 runs of NSGA-II. It can be observed that NSGA-II requires on average 22760 function evaluations to generate the approximate P-O solutions.

**Table 6** Statistical values of function evaluations obtained from 20 different runs of NSGA-II.

Best	worst	Mean	Median	Std. Dev.
12100	41200	22760	21550	7649.73

The bi-objective optimization formulation described in Section 4.2 is now solved for different values of  $p$  and  $(T_a - T_b)$ . Figure 13 shows the approximate P-O sets for different values of  $p$ , where  $(T_a - T_b)$  is kept  $75^\circ\text{C}$ . It can be observed from figure that by increasing  $p$ , the set of the approximate P-O solutions gets shifted away from the approximate P-O set of 0.1 MPa study. However, an improvement can be seen in the approximate P-O solutions for lower  $p$  than 0.1 MPa study. It is due to change in the thickness of shell and head. As  $p$  increases, the stresses developed in the pressure vessel also keep on increasing. To make the design safe, the thickness of the pressure vessel gets increased which can keep the stresses under  $S$ , but it increases  $TC$ .



**Fig. 13** Variation of  $\tau_{max}$  and  $TC$  at different internal pressure.

Figure 14 shows the approximate P-O sets for different  $(T_a - T_b)$  values, where  $p$  is kept 0.1 MPa. Similar observation can be seen from figure in which the thermal stresses increase with increase in temperature difference. These stresses are kept under  $S$  by increasing  $T_s$  and  $T_h$  values.

The post-processing of optimal data of bi-objective study for 0.1 MPa and temperature difference  $75^\circ\text{C}$  is also done in this paper. Figure 15 shows the optimal values of  $L$  and  $R$  of the pressure vessels corresponding to the approximate P-O solutions. It can be observed that solutions are grouped in two clusters. In cluster 1,

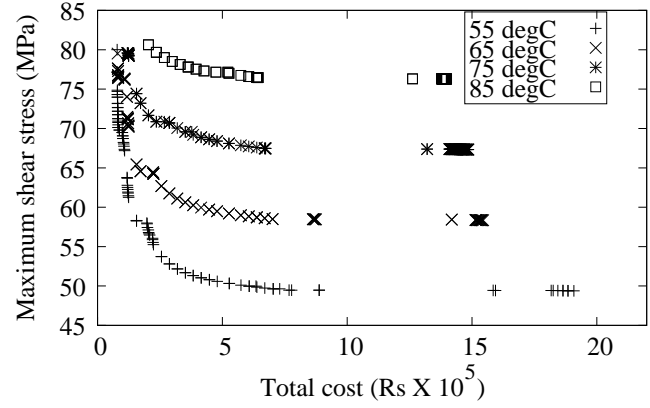


**Fig. 14** Variation of  $\tau_{max}$  and  $TC$  at different temperature difference.

$L$  varies from 550 mm to 600 mm and accordingly,  $R$  adjusts from 142 mm to 146 mm such that the volume constraint is satisfied. Similarly in cluster 2,  $L$  of pressure vessel shows a range from 123 mm to 156 mm for which  $R$  varies from 196 mm to 202 mm.

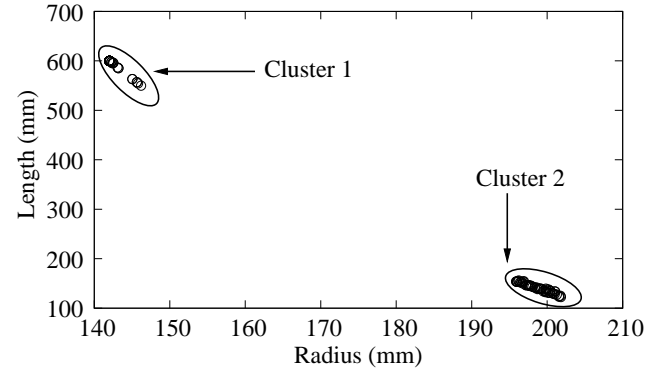


**Fig. 15** Optimal values of  $L$  and  $R$  at the approximate P-O set for 0.1 MPa internal pressure and  $75^\circ\text{C}$  temperature gradient.

Cluster 1 represents solutions with lower  $TC$  which can be observed from Fig. 16. It shows that  $TC$  varies from Rs  $1.23 \times 10^5$  to Rs  $6.73 \times 10^5$ . On the other hand,  $\tau_{max}$  varies from 67.5 MPa to  $S$  as shown in Fig. 17. In these figures, two solutions are marked as 1 and 2. These solutions have same radius and length, meaning that the volume is same for both solutions. However, solution 1 is safer than solution 2, whereas  $TC$  of solution 2 is less than solution 1. It is due to difference in the optimal values of thickness of shell and head as shown in Table 7. The pressure vessel design for solution 1 is thicker than solution 2 which reduces  $\tau_{max}$ . Since, the optimal head thickness of solution 1 is larger than solution 2, it increases  $TC$  of solution 1. On the other hand, solution 2 represents thinner pressure vessel which shows lower  $TC$  but  $\tau_{max}$  reaches to  $S$  limit. Rest of the solutions

show trade-off in the objective space with the above mentioned reason.

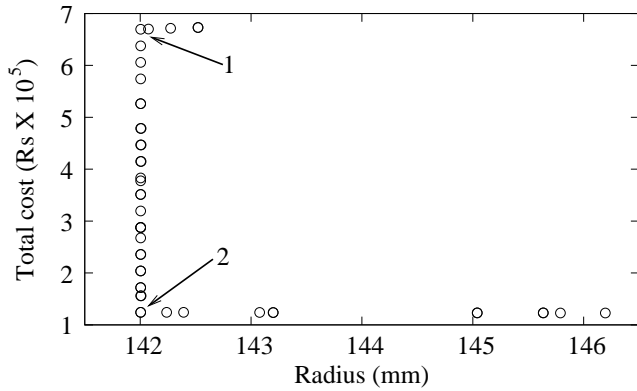


**Fig. 16** Optimal values of  $R$  with respect to their  $TC$  for cluster 1 approximate P-O set at 0.1 MPa internal pressure and 75°C temperature gradient.

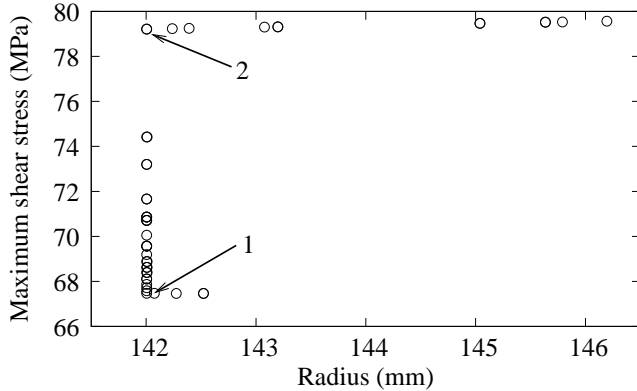


**Fig. 17** Optimal values of  $R$  with respect to their shear stress for cluster 1 approximate P-O set at 0.1 MPa internal pressure and 75°C temperature gradient.

**Table 7** Shell and head thickness for two solutions of same volume in cluster 1.

Solution	Shell thickness (mm)	Head thickness (mm)
1	5	34
2	3	3

It is noted that the difference between  $T_h$  and  $T_s$  for solution 1 in Table 7 is 29 mm. This difference can be avoided by including a constraint on thickness. However, it is not compulsory for the bi-objective optimization study as the differences in thicknesses of the P-O solutions can be observed from Fig. 18. The figure shows different ranges of  $(T_h - T_s)$  observed from the approximate P-O solutions. If any  $(T_h - T_s)$  value is desired,

then any solution from 0 mm to the desired thickness difference can be chosen.

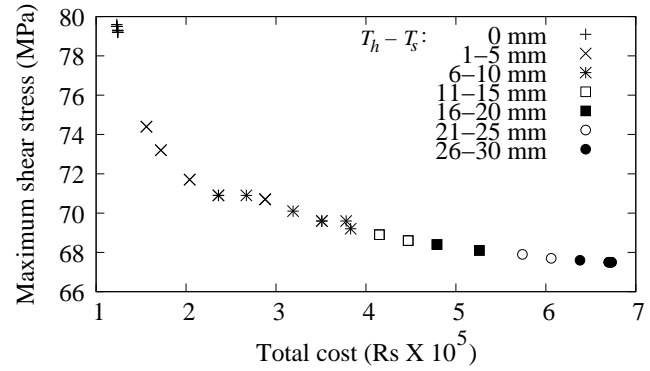


**Fig. 18** Differences in  $T_h$  and  $T_s$  for cluster 1 P-O solutions.

Cluster 2 represents solutions having lower  $\tau_{max}$  and higher  $TC$ . It can be observed from Fig. 19 that  $TC$  varies in the range of Rs  $13.22 \times 10^5$  to Rs  $14.9 \times 10^5$ , except two solutions. Similarly, almost all solutions shows  $\tau_{max}$  in the range of 67.3 MPa as shown in Fig. 20. In both figures, two solutions are marked as ‘3’ and ‘4’ which have same volume capacity.  $\tau_{max}$  is less for solution 3 because it is a thicker pressure vessel than solution 4 as shown in Table 8. Therefore,  $TC$  of solution 3 is more than solution 4. Similarly, solution 4 represents a thinner pressure vessel with lower  $TC$ , but  $\tau_{max}$  value reaches to  $S$ . In cluster 2 as well, a big difference between  $T_h$  and  $T_s$  is observed from Table 8. The ranges of differences in  $T_h$  and  $T_s$  for cluster 2 solutions are shown in Fig. 21. Here, majority of the cluster 2 P-O solutions show a difference of 40 mm between  $T_h$  and  $T_s$ .

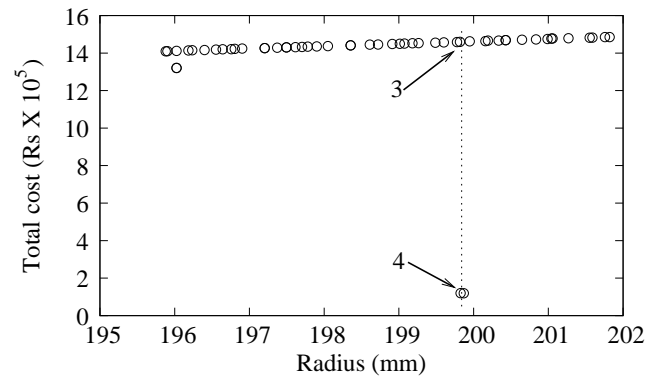


**Fig. 19** Optimal values of  $R$  with respect to their  $TC$  for cluster 2 approximate P-O set at 0.1 MPa internal pressure and 75°C temperature gradient.

It is interesting to note that solution 2 in Fig. 16 and solution 4 in Fig. 19 represent the cost effective pressure

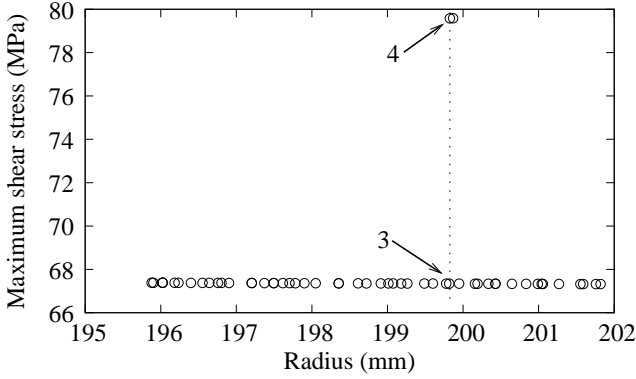


**Fig. 20** Optimal values of  $R$  with respect to their shear stress for cluster 2 approximate P-O set at 0.1 MPa internal pressure and 75°C temperature gradient.

**Table 8** Shell and head thickness for two solutions of same volume in cluster 2.

Solution	Shell thickness (mm)	Head thickness (mm)
3	5	45
4	3	3

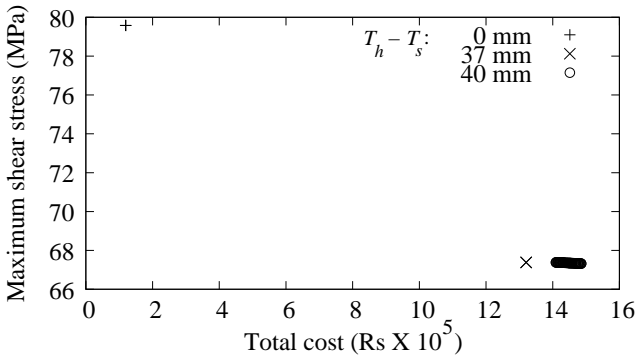


**Fig. 21** Differences in  $T_h$  and  $T_s$  for cluster 2 P-O solutions.

vessel design. Although the volume capacity of both of these solutions is same, but solution 2 has smaller radius and larger length than solution 4. This implies that the designer can even have different options for same cost and volume designs for relative comparison. This is another advantage offered by the bi-objective optimization over SOO.

If solutions 1 and 3 are compared in Figs. 17 and 20, both of them are the safest designs among other solutions. However,  $TC$  of solution 1 is much less than solution 3 as shown in Figs. 16 and 19. These two solutions represent either sides of knee region as discussed earlier. The marginal improvement in  $\tau_{max}$  for solution 3 drastically increases its  $TC$  with respect to solution 1.

## 5 Conclusions

In this paper, a pressure vessel was modeled for thermo-elastic loading by minimizing its  $TC$  and  $\tau_{max}$ . The combined effect due to internal pressure and temperature gradient was considered for a safe design. The two optimization methods were used to solve single-objective optimization problem, which generated similar optimal solutions. The perturbation analysis further supported the optimality of solution. From simulations, it was observed that  $\tau_{max}$  in a pressure vessel started increasing after the knee thickness due to increase in the compressive hoop/circumferential stress at the inner wall under thermo-elastic condition. FOS of a pressure vessel was also restricted around the knee thickness of the spherical head design. It can be concluded from this paper that material selection and other measures should be taken carefully for higher FOS pressure vessel under thermo-elastic condition. Later, the pressure vessel was designed using the bi-objective optimization which generated many approximate P-O solutions. Among these solutions, one extreme solution was equivalent to the optimal solution of SOO study, whereas other extreme solution generated with the equivalent knee thickness. These many trade-off solutions offered choice to the designer so that a relative comparison can be made in and out of the knee region for final design selection. The post-processing of the approximate P-O solutions showed that solutions were clustered into two groups representing minimum  $TC$  and minimum  $\tau_{max}$ . Based on the observation, any solution from cluster 1 can be preferred which can represent a cost effective, safe, and feasible  $T_h$  and  $T_s$  difference. Further trade-off was observed in these groups based on the pressure vessel thickness. In the future work, plane strain and transient temperature gradient conditions can be considered. Other optimization methods like PSO etc. can be used for better convergence. Moreover, GA can be coupled with other optimization methods to improve its convergence.

## A Attainment surface [14]

An approximate set  $A$  is called the  $k\%$  - approximate set of the empirical attainment function (EAD)  $\alpha_r(z)$ , iff it weakly dominates exactly those objective vectors that have been attained in at least  $k$  percentage of the  $r$  runs. Formally,  $\forall z \in Z : \alpha_r(z) \geq k/100 \Leftrightarrow A \preceq \{z\}$  where  $\alpha_r(z) = \frac{1}{r} \sum_{i=1}^r I(A^i \preceq \{z\})$ .  $A^i$  is the  $i$ th approximation set (run) of the optimizer and  $I(\cdot)$  is the indicator function, which evaluates to one if its argument is true and zero if its argument is false.

An attainment surface of a given approximate set  $A$  is the union of all tightest goals that are known to be attainable as a result of  $A$ . Formally, this is the set  $\{z \in \mathfrak{R}^n : A \preceq z \wedge \neg A \prec z\}$  [20].

## References

1. Chattopadhyay, S.: Pressure Vessels: Design and Practice. Mechanical and Aerospace Engineering Series. Taylor & Francis (2004)
2. Chun, S., Kim, Y.T., Kim, T.H.: A diversity-enhanced constrained particle swarm optimizer for mixed integer-discrete-continuous engineering design problems. *Advances in Mechanical Engineering* pp. 1–11 (2013)
3. Coelho, L.d.S., Mariani, V.C.: Use of chaotic sequences in a biologically inspired algorithm for engineering design optimization. *Expert Systems with Applications* **34**(3), 1905–1913 (2008)
4. Coello, C.A.C., Mezura-Montes, E.: Use of dominance-based tournament selection to handle constraints in genetic algorithms. In: *Proceedings of Intelligent Engineering Systems through Artificial Neural Networks*, vol. 11, pp. 177–182 (2001)
5. Deb, K.: An efficient constraint handling method for genetic algorithms. *Computer Methods in Applied Mechanics and Engineering* **186**(2-4), 311–338 (2000)
6. Deb, K.: *Multi-Objective Optimization using Evolutionary Algorithms*. Wiley: Chichester, UK (2001)
7. Deb, K., Agrawal, R.B.: Simulated binary crossover for continuous search space. *Complex Systems* **9**(2), 115–148 (1995)
8. Deb, K., Goyal, M.: A combined genetic adaptive search (genias) for engineering design. *Computer Science and Infomatics* **26**(4), 30–45 (1996)
9. Deb, K., Miettinen, K., Chaudhuri, S.: Toward an estimation of nadir objective vector using a hybrid of evolutionary and local search approaches. *Evolutionary Computation, IEEE Transactions on* **14**(6), 821–841 (2010)
10. Deb, K., Pratap, A., Agarwal, S., Meyarivan, T.: A Fast and Elitist Multiobjective Genetic Algorithm: NSGA-II. *Evolutionary Computation, IEEE Transactions on* **6**(2), 182–197 (2002)
11. Derrington, M.G.: The onset of yield in a thick cylinder subjected to uniform internal or external pressure and steady heat flow. *International Journal of Mechanical Sciences* **4**(1), 83–103 (1962)
12. Derrington, M.G., Johnson, W.: The onset of yield in a thick spherical shell subject to internal pressure and uniform heat flow. *Applied Scientific Research* **7**(6), 408–420 (1958)
13. Dimopoulos, G.G.: Mixed-variable engineering optimization based on evolutionary and social metaphors. *Computer Methods in Applied Mechanics and Engineering* **196**(4-6), 803–817 (2007)
14. Fonseca, C., Fonseca, V., Paquete, L.: Exploring the performance of stochastic multiobjective optimisers with the second-order attainment function. In: C. Coello Coello, A. Hernandez Aguirre, E. Zitzler (eds.) *Evolutionary Multi-Criterion Optimization, Lecture Notes in Computer Science*, vol. 3410, pp. 250–264. Springer Berlin Heidelberg (2005)
15. Gandomi, A.H., Yun, G.J., Yang, X.S., Talatahari, S.: Chaos-enhanced accelerated particle swarm optimization. *Communications in Nonlinear Science and Numerical Simulation* **18**(2), 327–340 (2013). URL <http://www.sciencedirect.com/science/article/pii/S1007570412003292>
16. Goldberg, D.E., Deb, K.: A comparative analysis of selection schemes used in genetic algorithms. In: *Foundations of Genetic Algorithms*, pp. 69–93. San Francisco, CA: Morgan Kaufmann (1991)
17. Hedar, A.R., Fukushima, M.: Derivative-free filter simulated annealing method for constrained continuous global optimization. *Journal of Global Optimization* **35**(4), 521–549 (2006)
18. Kannan, B.K., Kramer, S.N.: An augmented lagrange multiplier based method for mixed integer discrete continuous optimization and its applications to mechanical design. *Journal of Mechanical Design* **116**(2), 405–411 (1994)
19. Kayhan, A.H., Ceylan, H., Ayvaz, M.T., Gurarslan, G.: Psolver: A new hybrid particle swarm optimization algorithm for solving continuous optimization problems. *Expert Systems with Applications* **37**(10), 6798–6808 (2010)
20. Knowles, J., Thiele, L., Zitzler, E.: A Tutorial on the Performance Assessment of Stochastic Multiobjective Optimizers. TIK Report 214, Computer Engineering and Networks Laboratory (TIK), ETH Zurich (2006)
21. Knowles, J.D., Watson, R.A., Corne, D.: Reducing Local Optima in Single-Objective Problems by Multi-Objectivization. In: *Proceedings of the First International Conference on Evolutionary Multi-Criterion Optimization, EMO '01*, pp. 269–283. Springer-Verlag, London, UK (2001)
22. Lu, H.C.: A logarithmic method for eliminating binary variables and constraints for the product of free-sign discrete functions. *Discrete Optimization* **10**(1), 11–24 (2013)
23. MATLAB: version 6. The MathWorks Inc., Natick, Massachusetts (2006)
24. Mezura-Montes, E., Coello, C.A.C.: Useful infeasible solutions in engineering optimization. In: *Proceedings of the 4th Mexican International Conference on Artificial Intelligence*, vol. 3789, pp. 652–662 (2005)
25. Mezura-Montes, E., Coello Coello, C.A., Landa-Becerra, R.: Engineering optimization using simple evolutionary algorithm. In: *Tools with Artificial Intelligence, 2003. Proceedings. 15th IEEE International Conference on*, pp. 149–156. IEEE press (2003)
26. Moss, D.R.: *Pressure Vessel Design Manual*. Elsevier Science (2004)
27. Nahvi, H., Mohagheghian, I.: A particle swarm optimization algorithm for mixed variable nonlinear problems. *International Journal of Engineering* **24**, 65–78 (2011)
28. Noda, N., Hetnarski, R.B., Tanigawa, Y.: *Thermal Stresses*. Taylor and Francis (2003)
29. Parsopoulos, K.E., Vrahatis, M.N.: Unified particle swarm optimization for solving constrained engineering optimization problems. *Lecture Notes in Computer Science: Advances in Natural Computation* **3612**, 582–591 (2005)
30. Rao, S.S., Xiong, Y.: A hybrid genetic algorithm for mixed-discrete design optimization. *Journal of Mechanical Design* **127**(6), 1100–1112 (2005)
31. Sandgren, E.: Nonlinear integer and discrete programming in mechanical design optimization. *Journal of Mechanical Design* **112**(2), 223–229 (1990)
32. Sharma, D., Deb, K., Kishore, N.N.: Domain-Specific Initial Population Strategy for Compliant Mechanisms using Customized Genetic Algorithm. *Structural and Multidisciplinary Optimization* **43**(4), 541–554 (2011)
33. Sharma, D., Deb, K., Kishore, N.N.: Customized evolutionary optimization procedure for generating minimum weight compliant mechanisms. *Engineering Optimization* **46**(1), 39–60 (2014)
34. Sharma, H., Bansal, J.C., Arya, K.V.: Opposition based lévy flight artificial bee colony. *Memetic Computing* **5**(3), 213–227 (2013)
35. Solberg, I.: fminconset: <http://www.mathworks.in/matlabcentral/fileexchange/96fminconset> (2000)
36. Zahara, E., Kao, Y.T.: Hybrid neldermead simplex search and particle swarm optimization for constrained engineering design problems. *Expert Systems with Applications* **36**(2), 38803886 (2009)